A CFD INVESTIGATION OF Al$_2$O$_3$/WATER FLOW IN A DUCT HAVING BACKWARD-FACING STEP

R. Ekiciler[1,*], E. Aydeniz[2], K. Arslan[3]

ABSTRACT

Al$_2$O$_3$/water forced convection nanofluid flow was numerically studied in a duct with backward-facing step. Nanoparticle volume fraction was changed between 1%-5%. Diameter of nanoparticle was constant (d_p=40 nm). The Reynolds number was increased from 100 to 500. The step and total height of the duct were 4.8 mm and 9.6 mm, respectively. The bottom wall, which was positioned after the step, was heated with 2000 W/m^2 and the rest of the walls were adiabatic. Nusselt number, velocity profiles and friction factor were investigated in detail. It was obtained that Nusselt number increases with increasing nanoparticle volume fraction and Reynolds number.

Keywords: *Forced Convection, Nanofluid, Backward-facing Step, Laminar Flow, Diameter of Nanoparticle*

INTRODUCTION

Flow separation and reattachment of the fluid caused by sudden expansion is important in many engineering applications. Heat transfer applications of backward facing step (BFS) are mainly used in avionics systems, high performance heat exchangers, cooling of nuclear reactors, wide-angle diffusers, airfoils, electronic cooling equipment, cooling of turbine blades, combustion chambers, environmental control systems, axial and centrifugal compressors blade and is also used in many other heat transfer devices.

In the literature, the separation and reattachment flow over a backward-facing step was firstly carried out in the 1950's. Studies on separated flow have been researched more extensively by increasing popularity over in the last decade. Goldstein et al. [1] performed an experimental study to investigate the reattachment point under laminar and subsonic flow conditions over a step. They noticed that the reattachment point and boundary displacement thickness change with Reynolds number. Denham and Patrick [2] investigated 2D laminar flow over the BFS. Water was used as working fluid. The channel's expansion and aspect ratios are equal to 3 and 20, respectively. The Reynolds number was varied from 50 to 250. They observed that flow characteristics of BFS approximates to other 2D geometries having sudden expansion. Yet, both recirculation length and mass flow rate circulating were smaller. At Re=229, they noticed a fluctuation, which shows the beginning of transition to turbulent separated boundary layer. Rinoie et al. [3] experimentally investigated turbulent flow over the backward-facing step to clarify behavior of turbulent flow inside the reattachment shear layer using turbulent energy balance assisting in understanding of turbulent flow of BFS. Step height and aspect ratio were 0.02 m and 10, respectively. They observed that turbulent structures can be classified in three categories (the dead air, reversed flow and separated shear layer zone). In the turbulent energy balance, transverse diffusion assisting to balance the dissipation term was positive. Nie and Armally [4] examined numerically the effects of step height on heat transfer and flow characteristics in a three dimensional BFS channel. Flow was thought as laminar and forced convection conditions. Air was passed through the channel as working fluid. Thermo-physical properties of air were assumed constant along the channel. The study was performed at constant Reynold number (Re=343). Constant and uniform heat flux (q"w=50 W/m2) was subjected to downward of the step wall while the other walls were insulated. Three different step height was performed in this study. They observed at the end of the study that Nusselt number, general three- dimensional flow characteristic features, gradient locating in recirculation region increases with increasing step height. Also, they noticed that step height effects the friction coefficient distribution. Lan et al. [5] conducted numerical simulation of 3D turbulent forced convection flow in backward-facing step channel. Range of Reynolds number was at 20000-50000. The channel's step height and

expansion ratio was 4.8 and 1.48 mm, respectively. This study was done to understand the effects of Reynolds number and aspect ratio on heat transfer and fluid flow features. The Nusselt number, temperature, and general flow features distributions were presented. They concluded that Reynolds number and aspect ratio influence slightly flow separation and reattachment point but heat transfer is substantially influenced.

Nowadays, more and more energy is needed to supply energy of the World due to the developing technologies. Therefore, diversified heat transfer technologies have been set out to be developed. One of them is initiated by using nanofluids that are used for increasing heat transfer. Nanofluids are novel heat transfer fluids having nanoparticles whose sizes change from 1 nm to 100 nm suspended in the base fluids. In recent years nanofluids have been progressively studied. Abu- Nada [6] is the first researcher who conducted a numerical study concerning heat transfer by using nanofluids in ducts with backward-facing step. In this study, five different nanoparticles (CuO, Cu, TiO_2, Ag, and Al_2O_3) were used with volume fractions from 0.05% to 2.0%. Water was the base fluid. Duct was thought 2D and its expansion ratio was 2. The range of Reynolds number was 200-600. He reported that Nusselt number increases with increasing volume fractions. Al-aswadi et al. [7] studied numerically 2D laminar forced convection flow of nanofluids in channel with BFS. The base fluid was water. They conducted this study by using Al_2O_3, Au, Ag, CuO, TiO_2, Cu, SiO_2 and diamond nanoparticles with 0.05 volume fraction. The study was performed for Re=50, 100 and 175. Expansion ratio and step height and of the devised channel were 2 mm and 4.8 mm, respectively. All the walls were insulated. They presented the effects of Reynolds number and nanofluids types on pressure drop, velocity distribution and friction coefficient. They noticed that the highest wall shear stress is observed for SiO_2/water nanofluid. They found that nanofluids prepared nanoparticle with low density increase velocity much more compared to nanofluids prepared nanoparticle with high density. Also, they obtained that Reynolds number and skin friction coefficient are inversely proportional. Ekiciler and Arslan [8] numerically conducted a study of heat transfer and flow characterictics in forced convection laminar flow conditions by using 2D duct with BFS. SiO_2/water nanofluid was forced. The nanoparticle volume fraction was ranged from 1% to 4%. Reynolds number was selected from 75 to 225. Both of the step and inlet heights of the duct were 4.8 mm. As the downstream wall was subjected to constant and uniform heat flux of 2000 W/m^2, the other walls were insulated. It was found from the results of numerical simulation that the Nusselt number increases with increasing the nanoparticle volume fraction; however, there was no significant change on Darcy friction factor.

It is obvious from the above literature review that the case of forced convective heat transfer over BFS utilizing different nanoparticle volume fraction of Al_2O_3/water nanofluid seem have not been investigated in the past and this has motivated the present study. The present study deals with 2D laminar forced convective nanofluid flow over a BFS. Results of interests such as velocity distributions, Nusselt number, and friction factor for laminar forced convection over a horizontal BFS were reported to illustrate the effect of types of nanofluids on these parameters.

MATHEMATICAL MODELLING

Laminar forced heat transfer and flow of nanofluids in a 2D duct with BFS, which is presented in Figure 1, has been numerically investigated. The length of downstream and upstream wall were 0.05 m and 0.1 m, respectively. Total duct height was 9.6 mm. While downstream stepped wall was heated with uniform and constant heat flux of 2000 W/m2, the other walls were insulated. Solid particles with size under 100 nm were considered to be able to use single phase approach, thus single phase approach was practiced for nanofluid modeling and the phase of nanofluid was assumed to be as a continuous [9]. The following assumptions were adopted for this numerical study: (i) Both heat transfer and fluid flow in duct were in 2D and steady-state; (ii) fluid flow was incompressible and laminar flow; (iii) the physical properties of nanofluid, such as specific heat, density, thermal conductivity were taken as temperature independent; (iv) negligible viscous dissipation and radiation heat transfer; and (v) the base fluid and the nanoparticles were in thermal equilibrium.

With assumptions mentioned above, governing equations; continuity, momentum and energy are given below, respectively:

$$\vec{\nabla}.\vec{V} = 0$$

(1)

$$\rho \frac{D\vec{V}}{Dt} = -\Delta p + \mu \nabla^2 \vec{V} \tag{2}$$

$$\rho c_p \frac{DT}{Dt} = k \nabla^2 T \tag{3}$$
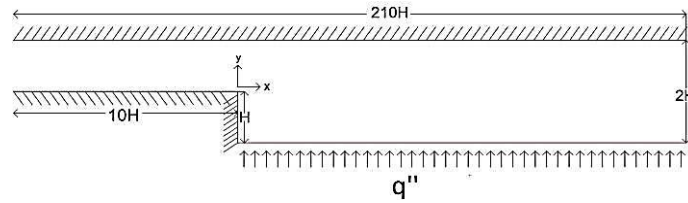
Figure 1. Schematic diagram for backward facing step

Table 2. Thermo-physical properties of nanoparticles and pure water

Types of Nanofluids	$\rho(kg/m^3)$	$\mu(N/ms)$	$k(W/mK)$	$Cp(kJ/kgK)$
Water	996.6	0.000855	0.613	4179
Al_2O_3 [10]	3970	-	40	765

Vajjha and Das [11] offered the equation of effective thermal conductivity for nanofluid as:

$$k_{eff} = k_{static} + k_{brownian} \tag{4}$$

Ghasemi and Aminossadati [12] presented the k_{static} as:

$$k_{static} = k_f \left[\frac{(k_s + 2k_f) - 2\varphi(k_f - k_s)}{(k_s + 2k_f) + \varphi(k_f - k_s)} \right] \tag{5}$$

where k_s and k_f are the thermal conductivies of the solid particles and the base fluid, respectively.

Vajjha and Das [11] presented thermal conductivity originating from Brownian motion as:

$$k_{brownian} = 5 \times 10^4 \beta \varphi \rho_f c_{pf} \sqrt{\frac{KT}{\rho_s d_p}} f(T, \varphi) \tag{6}$$

where;

$$f(T, \varphi) = (2.8217 \times 10^{-2} \varphi + 3.917 \times 10^{-3}) \frac{T}{T_r} + (-3.0669 \times 10^{-2} \times 10^{-2} \varphi - 3.91123 \times 10^{-3}) \tag{7}$$

where T is the fluid temperature and taking constant at 300 K, K is the Boltzmann constant and T_r is the reference temperature.

Corcione [13] suggested the equation of effective thermal expansion for nanofluid as:

$$\beta_{eff} = \frac{(1-\varphi)(\rho\beta)_f + \varphi(\rho\beta)_s}{(1-\varphi)\rho_f + \varphi\rho_s} \tag{8}$$

where β_s and β_f are the thermal expansion of nanoparticles and base fluid, respectively.

Table 3. β value of different nanoparticles and its boundary conditions

Parameters	Al$_2$O$_3$
β	$8.4407(100\ \varphi\ )^{-1.07304}$ [11]
Concentration	$1\% \leq \varphi \leq 4\%$
Temperature	298 K≤T≤363 K

Corcione [13] presented viscosity of nanofluid as:

$$\frac{\mu_{eff}}{\mu_f} = \frac{1}{1 - 34.87(d_p / d_f)^{-0.3} \varphi^{1.03}} \tag{9}$$

where;

$$d_f = \left[\frac{6M}{N\pi\rho_{fo}} \right]^{1/3} \tag{10}$$

where μ_f and μ_{eff} are viscosity of base fluid and nanofluid, respectively. φ is volume fraction of nanofluid, d_f is the base fluid equivalent diameter and d_p is diameter of nanoparticle., M is the base fluid's moleculer weight, N is the Avogadro number and ρ_{fo} is the mass density of the base fluid calculated at T=293 K.

Corcione [13] proposed the effective density of nanofluid as:

$$\rho_{eff} = (1-\varphi)\rho_f + \varphi\rho_s \tag{11}$$

where ρ_s, ρ_f and ρ_{eff} are densities of nanoparticle, base fluid and nanofluid, respectively.

Corcione [13] offered the effective specific heat of nanofluid as:

$$\left(c_p\right)_{eff} = \frac{(1-\varphi)(\rho c_p)_f + \varphi(\rho c_p)_s}{(1-\varphi)\rho_f + \varphi\rho_s} \tag{12}$$

where c_{pf} and c_{ps} are the specific heat of base fluid and nanoparticles, respectively.

Average Nusselt number, Darcy friction factor and heat transfer coefficient are calculated as:

$$Nu = \frac{hD_h}{k} \tag{13}$$

$$f = \frac{\Delta P(D_h / L)}{\rho u_i^2 / 2} \qquad (14)$$

$$h = \rho u_i A_c c_p (T_o - T_i) / A_s (T_w - T_m) \qquad (15)$$

NUMERICAL PROCEDURE AND MESH INDEPENDENCE TEST

In the numerical computations, the finite-volume method based commercial CFD software Ansys Fluent 17.0 was used to perform the numerical calculations by solving the governing equations along with the boundary conditions. The convection terms in mass, momentum and energy equations were discretized using a second order upwind scheme. The standard scheme was employed for discretization of pressure and the SIMPLE algorithm was used to resolve the coupling between velocity and pressure. The Green-Gauss cell based method was applied for discretization of the momentum and energy equations. To obtain convergence, each equation for mass, momentum, and energy were iterated until the residual falls below 1×10^{-6}. No convergence problems were observed during the calculations. The hexahedral mesh distribution was used for the duct with BFS. The numbers of mesh points or control volumes were increased close to the wall of the duct and near to the BFS to enhance the resolution and accuracy as given in Figure 2.
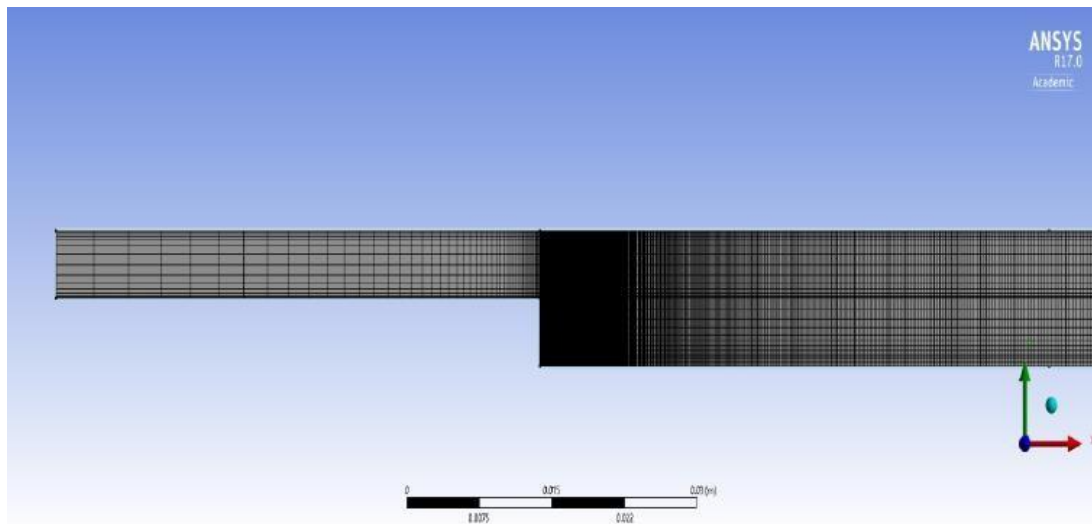

Figure 2. Mesh distribution of the computational domain

The mesh independence study was performed by refining the mesh number until the variation in both average Nusselt number and average friction factor were less than 0.1%. To obtain the optimum mesh number, a grid independence study was conducted using fifteen different mesh numbers changing from 6.2×10^2 to 1.5×10^5 for Re=500. Changing of Nusselt number and average friction factor values with mesh number for pure water flow is given in Figure 3 as an illustration. It was observed that a further refinement of mesh number from 9×10^3 to 1.5×10^5, the changing of average Nusselt number and average friction factor is negligible. Hence, optimum mesh number with minimum computational time and maximum accuracy approximately can be seen at 2.6×10^4 for this study.
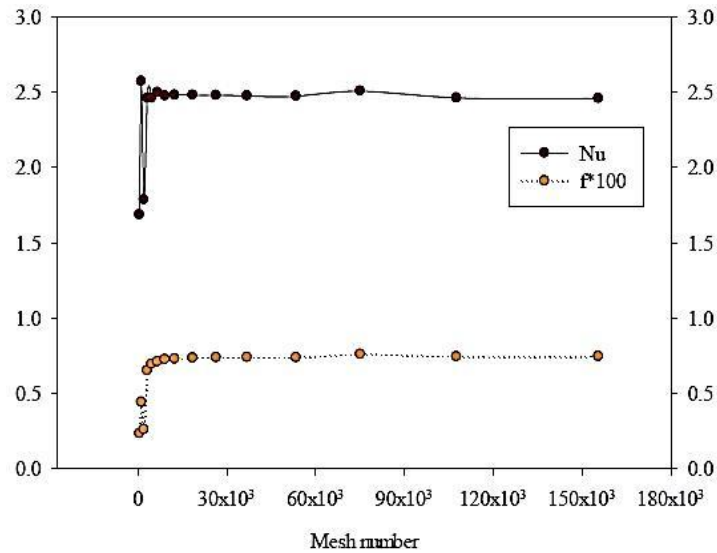
Figure 3. Mesh independence study for Nusselt number and friction factor at Re=500

To understand the accuracy of the numerical simulation, values of average pressure was compared with a study conducted by Al-aswadi et al. [7] obtained from literature in Figure 4. The results obtained by present study are good agreement with the study conducted by Al-aswadi et al. [7].
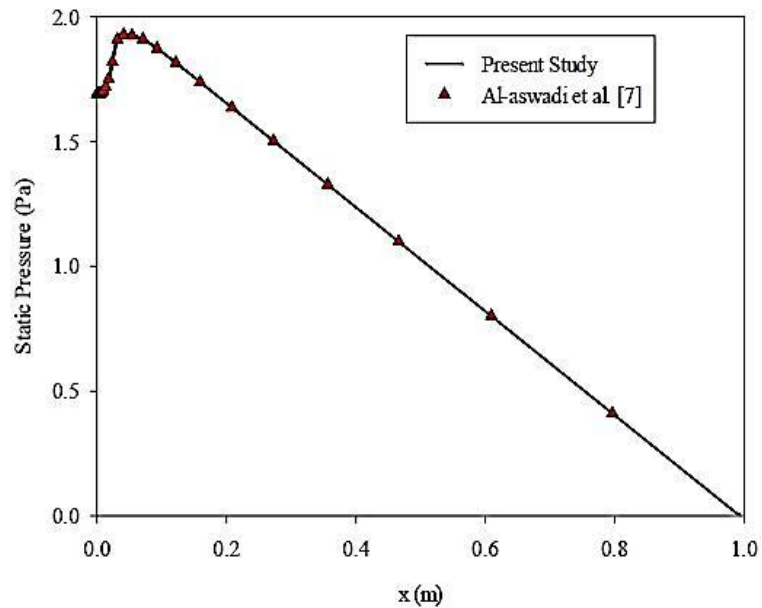
**Figure 4.** Comparison of pressure drop of the present results for pure water at Re=175

RESULTS AND DISCUSSION

Velocity distribution of Al_2O_3/water nanofluid for different nanoparticle volume fraction is presented at Re=400 in Figure 5. It can be seen from the figure that nanoparticle volume fraction has an active role in velocity distribution. Velocity magnitude increases with increasing the nanoparticle volume fraction. The highest velocity distribution of Al_2O_3/water nanofluid is at 5% volume fraction. Figure 5(a) and Figure 5(b) testimony that there is a recirculation region occurs after the step. Figure 5(c), Figure 5(d), and Figure 5(e) show that the nanofluid flow is independent of effect of sudden expansion.
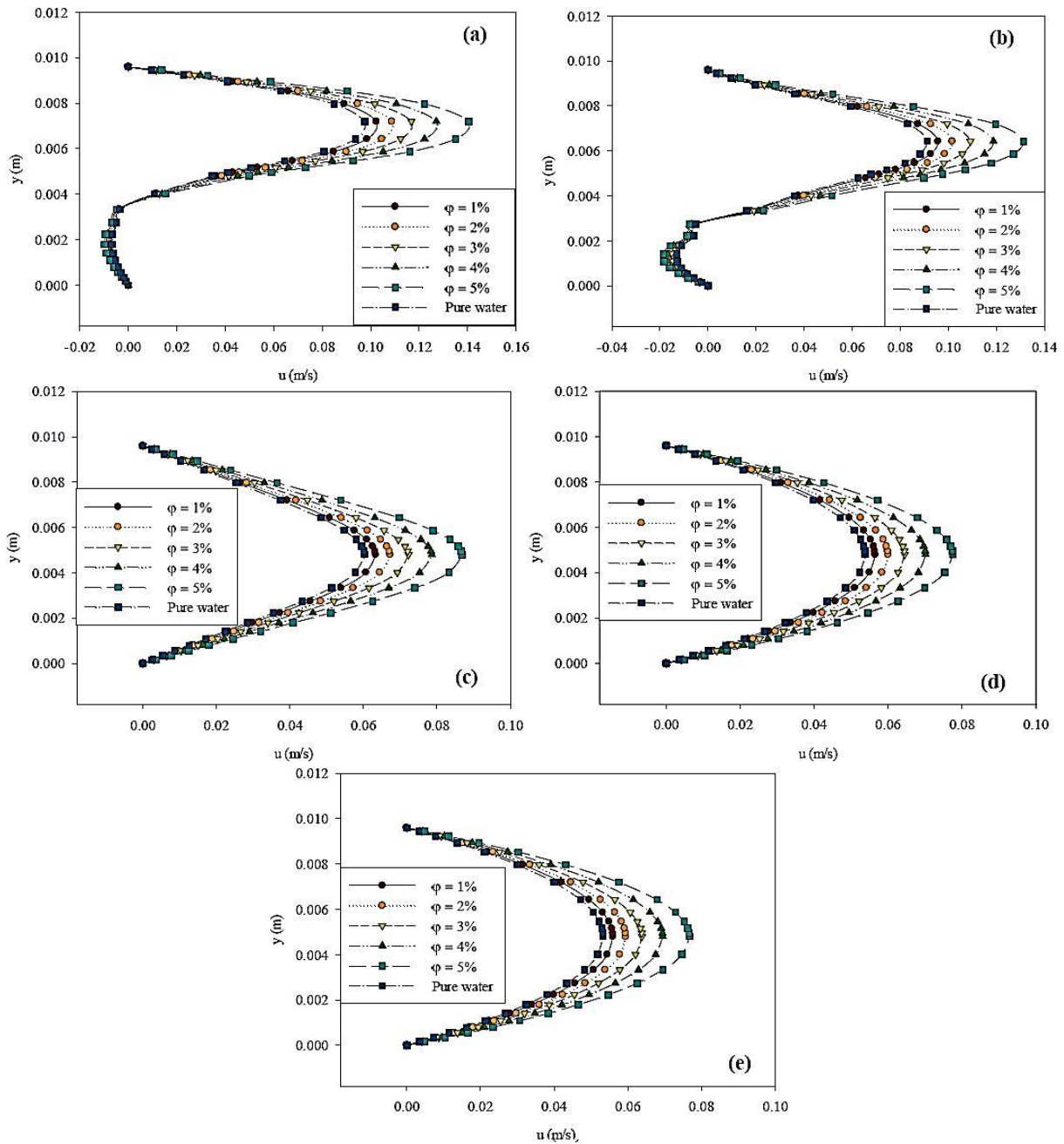
Figure 5. The effects of nanoparticle volume fraction on velocity distribution using Al$_2$O$_3$/water at Re=400 for different locations; (a) x=0.01 m, (b) x=0.03 m, (c) x=0.13 m, (d) x=0.35 m, (e) x=1.0 m

Figure 6 shows average Nusselt number distribution of Al$_2$O$_3$/water nanofluid and pure water as a function of Reynolds number. The nanoparticle volume fraction is changed from 1% to 5%. It realized that Nusselt number increases with increasing Reynolds number. Al$_2$O$_3$/water nanofluid having 5% volume fraction has the highest Nusselt number while pure water has the lowest one. This result demonstrates that Al$_2$O$_3$/water nanofluid flow enhances the heat transfer.
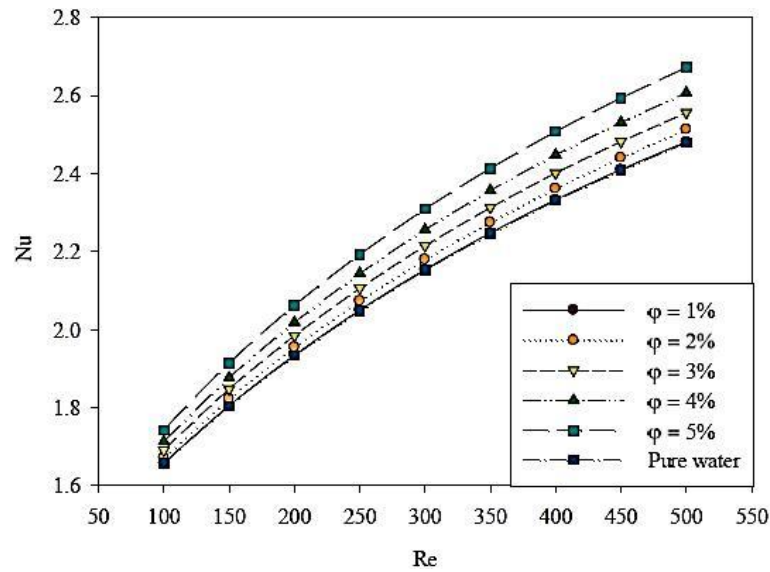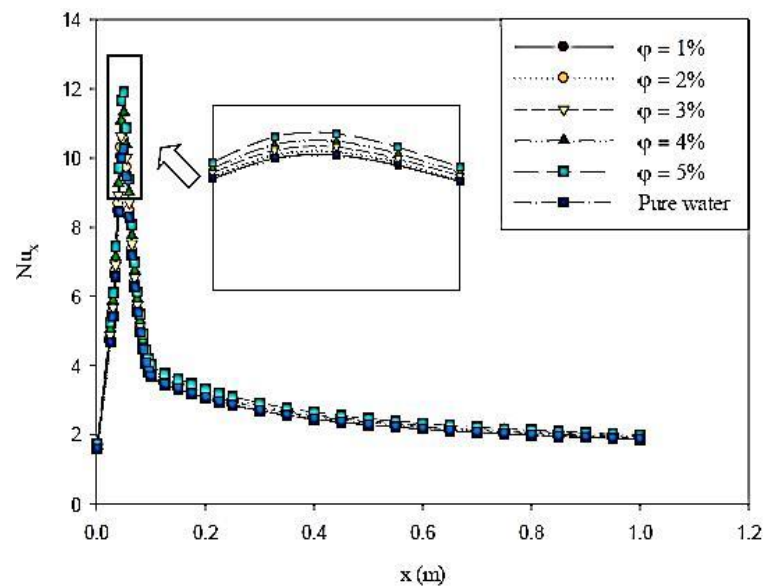
Figure 6. Average Nusselt number distribution using Al_2O_3/water nanofluid and pure water for different nanoparticle volume fractions

The effect of nanoparticle volume fraction on average friction factor distribution of Al_2O_3/water nanofluid and pure water is given in Figure 7. It is revealed that average friction factor decreases with Reynolds number for all nanoparticle volume fractions. In addition, average friction factor does not almost influence by nanoparticle volume fractions, which is the results with Ref. [14].
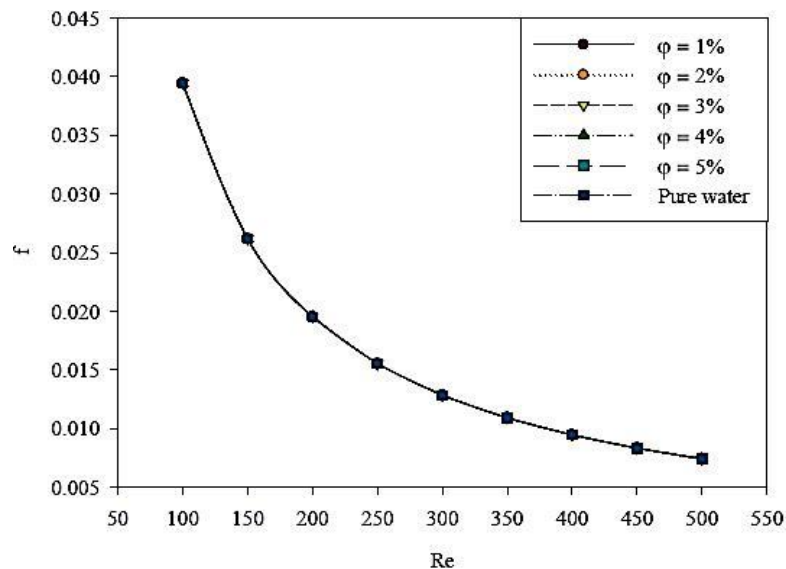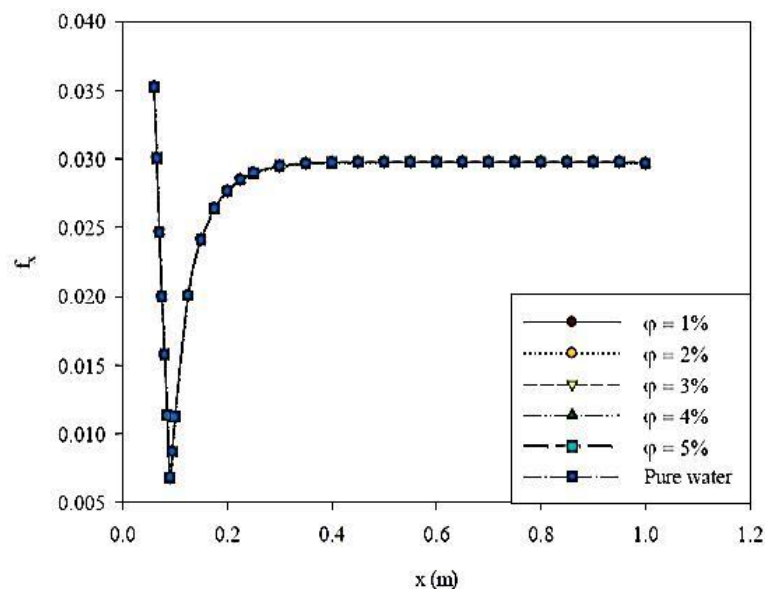

Figure 7. Average friction factor distribution using Al_2O_3/water nanofluid and pure water for different nanoparticle volume fractions

The local Nusselt number distribution is presented along the heated wall for Re=400 in Figure 8. It is noticed that the local Nusselt number increases substantially to its maximum value which is obtained at the separation point. After that it decreases until the reattachment point and then it takes almost a fixed shape, when the flow is being thermally fully developed condition. Moreover, local Nusselt number distribution presents the same characteristic behavior for all nanoparticle volume fractions. Local Nusselt number increases with increasing CuO nanoparticle volume fraction, also. Maximum local Nusselt number can be obtained at 4.0% nanoparticles volume fraction for Re=400.

Figure 8. Local Nusselt number distribution using Al_2O_3/water nanofluid and pure water for different nanoparticle volume fractions at Re=400

The local Darcy friction factor distribution is illustrated along the heated wall different nanoparticle volume fractions and Re=400 in Figure 9. It is noticed that the local Darcy friction factor decreases and then increases until it reaches a point where remains constant along the rest of heated wall. This shows that the local Darcy friction factor approaches the hydrodynamically fully developed condition. Also, it is realized that the average Darcy friction factor is independent from nanoparticle volume fraction.

Figure 9. Local friction factor distribution using Al_2O_3/water nanofluid and pure water for different nanoparticle volume fractions at Re=400

CONCLUDING REMARKS

Al_2O_3/water nanofluid over two-dimensional backward- facing step is simulated under laminar forced convection condition. As a result, Al_2O_3/water nanofluid enhances heat transfer. The average Nusselt number

increases with increasing the Reynolds number and nanoparticle volume fraction. Also, Darcy friction factor decreases with increasing Reynolds number. There is no effect of changing of nanoparticle volume fractions on average Darcy friction factor.

NOMENCLATURE

c_p	Specific heat [J/kg K]
D_h	Hydraulic diameter, 2h [m]
d_p	Nanoparticles diameter [nm]
ER	Expansion ratio, ER= h/H
F	Average friction factor
h	Inlet channel height [m]
H	Total channel height [m]
K	Boltzmann constant
K	Thermal conductivity [W/m K]
L	Length of the heated section [m]
L_S	The length of step [m]
M	Molecular weight [kg/kmol]
N	Avogadro number
Nu	Average Nusselt number, hD_h/k
q"	Heat flux [W/m^2]
P	Pressure [Pa]
Re	Reynolds number, $\rho u_i D_h/\mu$
S	Step height, [nm]
T	Fluid temperature [K
u	Velocity component on x direction [m/s]
v	Velocity component on y direction [m/s]
w	Velocity component on z direction [m/s]
Φ	Nanoparticle volume fraction
B	Thermal expansion coefficient [1/K]
ρ	Density [kg/m^3]
μ	Dynamic viscosity [N s/m^2]
τ_w	Wall shear stress [N/m^2]
υ	Kinematic viscosity [m^2/s]
eff	Effective
f	Fluid
s	Solid
nf	Nanofluid
w	Wall
i	Inlet condition
o	Outlet condition
x	Local
c	Cross-section

r   Reference

REFERENCES

[1] Goldstein, R. J., Eriksen, V. L., Olson, R. M., & Eckert, E. R. G. (1970). Laminar separation, reattachment, and transition of the flow over a downstream-facing step. Journal of Basic Engineering, 92(4), 732-739.

[2] Denham, M. K., Patrick, M. A. (1974). Laminar flow over a downstream-facing step in a two-dimensional flow channel. Transactions of the American Institute of Chemical Engineers 52(4), 361-367.

[3] Rinoie, K., Shirai, Y., Saitao, Y., Sunada, Y. (1998) Behaviours of separated and reattaching flow formed over backward-facing step. 21st ICAS Congress.

[4] Nie, J. H., Armaly, B. F. (2002). Three-dimensional convective flow adjacent to backward-facing step-effects of step height. International journal of heat and mass transfer, 45(12), 2431-2438.

[5] Lan, H., Armaly, B. F., Drallmeier, J. A. (2009). Three-dimensional simulation of turbulent forced convection in a duct with backward-facing step. International Journal of Heat and Mass Transfer, 52(7-8), 1690-1700.

[6] Abu-Nada, E. (2008). Application of nanofluids for heat transfer enhancement of separated flows encountered in a backward facing step. International Journal of Heat and Fluid Flow, 29(1), 242-249.

[7] Al-Aswadi, A. A., Mohammed, H. A., Shuaib, N. H., Campo, A. (2010). Laminar forced convection flow over a backward facing step using nanofluids. International Communications in Heat and Mass Transfer, 37(8), 950-957.

[8] Ekiciler, R., Arslan, K. (2016) Numerical analysis of SiO_2/water nanofluid flow over backward facing step. International Conference of Engineering and Natural Sciences pp 331–339.

[9] Moraveji, M. K., Darabi, M., Haddad, S. M. H., Davarnejad, R. (2011). Modeling of convective heat transfer of a nanofluid in the developing region of tube flow with computational fluid dynamics. International communications in heat and mass transfer, 38(9), 1291-1295.

[10] Salman, B. H., Mohammed, H. A., Kherbeet, A. S. (2012). Heat transfer enhancement of nanofluids flow in microtube with constant heat flux. International Communications in Heat and Mass Transfer, 39(8), 1195-1204.

[11] Vajjha, R. S., Das, D. K. (2009). Experimental determination of thermal conductivity of three nanofluids and development of new correlations. International Journal of Heat and Mass Transfer, 52(21-22), 4675-4682.

[12] Ghasemi, B., & Aminossadati, S. M. (2010). Brownian motion of nanoparticles in a triangular enclosure with natural convection. International Journal of Thermal Sciences, 49(6), 931-940.

[13] Corcione, M. (2010). Heat transfer features of buoyancy-driven nanofluids inside rectangular enclosures differentially heated at the sidewalls. International Journal of Thermal Sciences, 49(9), 1536-1546.

[14] Ekiciler, R., & Arslan, K. (2018). CuO/Water Nanofluid Flow over Microscale Backward-Facing Step and Analysis of Heat Transfer Performance. Heat Transfer Research, 49(15).